ЖЭТФ, 2010, том 137, вып. 2, стр. 368–379

TWO-DIMENSIONAL ANDERSON–HUBBARD MODEL IN THE DMFT+Σ APPROXIMATION

***E. Z. Kuchinskii*[*], *N. A. Kuleeva, I. A. Nekrasov, M. V. Sadovskii*[**]**

Institute for Electrophysics, Russian Academy of Sciences
620016, Ekaterinburg, Russia

Received August 26, 2009

The density of states, the dynamic (optical) conductivity, and the phase diagram of the paramagnetic two-dimensional Anderson–Hubbard model with strong correlations and disorder are analyzed within the generalized dynamical mean field theory (DMFT+Σ approximation). Strong correlations are accounted by the DMFT, while disorder is taken into account via the appropriate generalization of the self-consistent theory of localization. We consider the two-dimensional system with the rectangular "bare" density of states (DOS). The DMFT effective single-impurity problem is solved by numerical renormalization group (NRG). The "correlated metal", Mott insulator, and correlated Anderson insulator phases are identified from the evolution of the density of states, optical conductivity, and localization length, demonstrating both Mott–Hubbard and Anderson metal–insulator transitions in two-dimensional systems of finite size, allowing us to construct the complete zero-temperature phase diagram of the paramagnetic Anderson–Hubbard model. The localization length in our approximation is practically independent of the strength of Hubbard correlations. But the divergence of the localization length in a finite-size two-dimensional system at small disorder signifies the existence of an effective Anderson transition.

1. INTRODUCTION

The study of disordered electronic systems with the account of interaction effects is one of the central problems of the modern condensed matter theory [1]. According to the scaling theory of localization [2], there is no metallic state in two-dimensional (2D) systems, with all the electronic states localized at the smallest possible disorder. This prediction was first made for noninteracting 2D systems, and soon after it was shown that the weak electron-electron interaction enhances localization in most cases [3]. Experiments performed in the early 1980s on different 2D systems [4] essentially confirmed these predictions. However, some theoretical works produced an evidence of a rather different possibility [5] for 2D systems to evolve to the state with an infinite metallic-like conductivity at zero temperature in case of weak disorder and sufficiently strong correlations. Experimental observation of a metal–insulator transition (MIT) in 2D systems with weak enough disorder but strong correlations (low electronic densities) [6], which apparently contradicted the predictions of the scaling theory of localization, stimulated extensive theoretical studies, with no commonly accepted solution up to now (see the review in Ref. [7]).

One of the basic models allowing a simultaneous account of both strong enough electronic correlations, leading to the Mott MIT [8], and effects of strong disorder, leading to the Anderson MIT [9], is the Anderson–Hubbard model, intensively studied in recent years [10–16].

In Refs. [10–12], the three-dimensional (3D) Anderson–Hubbard model was analyzed using dynamical mean field theory (DMFT), which is extensively used in the theory of strongly correlated electrons [17–20]. However, disorder effects were mostly taken into account via the average density of states and the coherent potential approximation (CPA) [21, 22], which misses the effects of Anderson localization. To overcome this problem, Dobrosavljević and Kotliar [10] have proposed the DMFT approach, where the solution of self-consistent stochastic DMFT equations were used to calculate the geometrically averaged local density of states. This approach was further developed in Refs. [11, 12] with the DMFT account for Hubbard correlations, which led to a highly nontrivial phase diagram of the 3D paramagnetic Anderson–Hubbard model [12], containing the correlated metal,

[*]E-mail: kuchinsk@iep.uran.ru
[**]E-mail: sadovski@iep.uran.ru

Mott insulator, and correlated Anderson insulator phases. However, the major problem of the approach in Refs. [10–12] is its practical inability of direct calculations of conductivity, which actually determines the MIT itself.

In our previous work [13], we have studied the 3D paramagnetic Anderson–Hubbard model using our recently developed DMFT+Σ approximation [23–26], which preserves the standard single-impurity DMFT approach, taking the local Hubbard correlations into account, allowing the use of the standard "impurity solvers" like NRG [27–29], at the same time allowing the inclusion of additional (local or nonlocal) interactions. Strong disorder was accounted for via some generalization of the self-consistent theory of localization [30–35]. In the framework of this approach, we have been able not only to reproduce the phase diagram qualitatively similar to that obtained in Ref. [12] but also to calculate the dynamic (optical) conductivity for a wide frequency range.

In Ref. [15], the Hubbard–Anderson model was studied for both 3D and 2D systems. As the main mechanism leading to delocalization, a kind of "screening" of the random (disorder) potential by a local Hubbard interaction was introduced [14]. Then the Anderson–Hubbard model was reduced to an effective single-particle Anderson model with a renormalized distribution of local site energies, which was calculated in the atomic limit. All the other effects of electron correlations were neglected. Strong disorder effects were accounted for within the self-consistent theory of localization. In this approach, the authors obtained a significant increase in the localization length with an increase in the Hubbard interaction in 2D. However, the localization length itself remained finite, the system being localized at smallest possible disorder, and hence the Anderson transition in 2D was still absent. Similar results were also obtained in numerical simulations of the 2D Anderson–Hubbard model in Ref. [16].

In this paper, we directly generalize the method in Ref. [13] to the case of 2D systems. We use the DMFT+Σ approach to calculate the DOS, optical conductivity, and localization length and to construct the phase diagram of the 2D paramagnetic Anderson–Hubbard model with strong electronic correlations and strong disorder. Strong correlations are taken into account via DMFT, while disorder effects are treated by the appropriate generalization of the self-consistent theory of localization.

The paper is organized as follows. In Sec. 2, we briefly describe our DMFT+Σ approximation in application to the disordered Hubbard model. In Sec. 3, we formulate the basic DMFT+Σ expressions for the optical conductivity and the self-consistency equation for the generalized diffusion coefficient. Our results for the DOS, optical conductivity, and localization length are given in Sec. 4, where we also analyze the phase diagram of the 2D disordered Hubbard model and briefly discuss the optical sum rule within our approach. Finally, we present a short conclusion, which includes the discussion of problems yet to be solved.

2. BASICS OF THE DMFT+Σ APPROACH

In what follows, we consider the paramagnetic disordered Anderson–Hubbard model at half-filling for arbitrary correlations and disorder. This model treats both the Mott–Hubbard and Anderson MIT on the same footing. The Hamiltonian of the model can be written as

$$H = -t \sum_{\langle ij \rangle \sigma} a^{\dagger}_{i\sigma} a_{j\sigma} + \sum_{i\sigma} \epsilon_i n_{i\sigma} + U \sum_i n_{i\uparrow} n_{i\downarrow}, \quad (1)$$

where $t > 0$ is the nearest-neighbor transfer integral, U is the local Hubbard repulsion, $n_{i\sigma} = a^{\dagger}_{i\sigma} a_{i\sigma}$ is the electron number operator at a given site i, $a_{i\sigma}$ ($a^{\dagger}_{i\sigma}$) is the annihilation (creation) operator for an electron with spin σ, and the local energies ϵ_i are assumed to be randomly and independently distributed over different lattice sites. To simplify the diagram technique in what follows, we assume the ϵ_i distribution to be Gaussian,

$$\mathcal{P}(\epsilon_i) = \frac{1}{\sqrt{2\pi}\Delta} \exp\left(-\frac{\epsilon_i^2}{2\Delta^2}\right), \quad (2)$$

where Δ is a disorder parameter and the Gaussian random field ("white" noise) of energy levels ϵ_i at different lattice sites induces "impurity"-like scattering, leading to the standard diagram technique for calculations of the averaged Green's functions [35].

The DMFT+Σ approach, initially proposed in Refs. [23–26] as a simple method to include nonlocal interactions (fluctuations) into the standard (local) DMFT scheme, is also very convenient for taking any additional interaction (local or nonlocal) of arbitrary nature into account in the DMFT.

In the DMFT+Σ approximation, we choose the single-particle Green's function in the form

$$G_{\mathbf{p}}(\varepsilon) = \frac{1}{\varepsilon + \mu - \varepsilon(\mathbf{p}) - \Sigma(\varepsilon) - \Sigma_{\mathbf{p}}(\varepsilon)}, \quad (3)$$

where $\varepsilon(\mathbf{p})$ is the "bare" electron spectrum, $\Sigma(\varepsilon)$ is the local (DMFT) self-energy due to Hubbard interactions,

and $\Sigma_{\mathbf{p}}(\varepsilon)$ is an "external" (in general case, momentum dependent) self-energy due to some other interaction. The main assumption of our approach (both its advantage and deficiency) is precisely in this additive form (neglecting the interference effects) of the total self-energy in (3) [23–26], which allows retaining the standard form of self-consistent DMFT equations [20] with two major generalizations. First, at each iteration of the DMFT loop, we recalculate the "external" self-energy $\Sigma_{\mathbf{p}}(\mu, \varepsilon, [G_{\mathbf{p}}(\varepsilon)])$ within some (approximate) scheme, taking the "external" interaction into account (in the present case, the interaction due to disorder scattering). Second, the local Green's function for an effective DMFT impurity problem is defined as

$$G_{ii}(\varepsilon) = \frac{1}{N}\sum_{\mathbf{p}} \frac{1}{\varepsilon + \mu - \varepsilon(\mathbf{p}) - \Sigma(\varepsilon) - \Sigma_{\mathbf{p}}(\varepsilon)} \qquad (4)$$

at each step of the standard DMFT procedure. Finally, we obtain the desired Green's function in form (3), where $\Sigma(\varepsilon)$ and $\Sigma_{\mathbf{p}}(\varepsilon)$ are self-energies obtained at the end of our iteration procedure.

For $\Sigma_{\mathbf{p}}(\varepsilon)$ appearing due to disorder scattering, we use the simple one-loop contribution, neglecting diagrams with "crossing" interaction lines, i. e., the self-consistent Born approximation [35], which in the case of Gaussian disorder (2) leads to the usual expression

$$\Sigma_{\mathbf{p}}(\varepsilon) = \Delta^2 \sum_{\mathbf{p}} G(\varepsilon, \mathbf{p}) \equiv \Sigma_{imp}(\varepsilon), \qquad (5)$$

with the "external" self-energy being $\mathbf{p}$-independent (local) in this case.

3. OPTICAL CONDUCTIVITY IN THE DMFT+Σ APPROACH

It is obvious that calculations of optical (dynamic) conductivity provide the direct way to study the MIT because the frequency dependence of conductivity, as well as its static value at zero frequency of an external field, allows making a clear distinction between the metallic and insulating phases (at $T = 0$).

A local nature of the irreducible self-energy in DMFT allows reducing the calculation of optical conductivity to the calculation of the usual particle–hole loop without DMFT vertex corrections due to the local Hubbard interaction [13, 26]. The final expression for the real part of the optical conductivity obtained in this way in Refs. [13, 26] takes the form

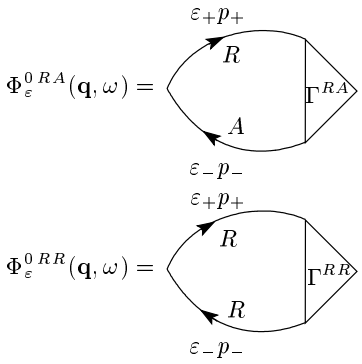

Fig. 1. Diagram representation of $\Phi_\varepsilon^{0RA}(\mathbf{q},\omega)$ and $\Phi_\varepsilon^{0RR}(\mathbf{q},\omega)$

$$\mathrm{Re}\,\sigma(\omega) = \frac{e^2\omega}{2\pi}\int\limits_{-\infty}^{\infty} d\varepsilon\,[f(\varepsilon_-) - f(\varepsilon_+)] \times$$
$$\times\,\mathrm{Re}\left\{\phi_\varepsilon^{0RA}(\omega)\left[1 - \frac{\Sigma^R(\varepsilon_+) - \Sigma^A(\varepsilon_-)}{\omega}\right]^2 - \right.$$
$$\left. - \phi_\varepsilon^{0RR}(\omega)\left[1 - \frac{\Sigma^R(\varepsilon_+) - \Sigma^R(\varepsilon_-)}{\omega}\right]^2\right\}, \qquad (6)$$

where $f(\varepsilon)$ is Fermi distribution, $\varepsilon_\pm = \varepsilon \pm \omega/2$, and

$$\phi_\varepsilon^{0RR(RA)}(\omega) =$$
$$= \lim_{q\to 0}\frac{\Phi_\varepsilon^{0RR(RA)}(\omega,\mathbf{q}) - \Phi_\varepsilon^{0RR(RA)}(\omega,0)}{q^2}, \qquad (7)$$

where we introduce two-particle loops

$$\Phi_\varepsilon^{0RR(RA)}(\omega,\mathbf{q}) = \sum_{\mathbf{p}} G^R(\varepsilon_+,\mathbf{p}_+)G^{R(A)}(\varepsilon_-,\mathbf{p}_-) \times$$
$$\times\,\Gamma^{RR(RA)}(\varepsilon_-,\mathbf{p}_-;\varepsilon_+,\mathbf{p}_+), \qquad (8)$$

represented diagrammatically in Fig. 1 with $\mathbf{p}_\pm = \mathbf{p} \pm \mathbf{q}/2$ and with the R and A superscripts corresponding to retarded and advanced Green's functions. The vertices $\Gamma^{RR(RA)}(\varepsilon_-,\mathbf{p}_-;\varepsilon_+,\mathbf{p}_+)$ contain all vertex corrections due to disorder scattering, but do not include vertex corrections due to the Hubbard interaction.

The problem is thus much simplified. To calculate the optical conductivity in the DMFT+Σ approximation, we only have to solve a single-particle problem to determine the local self-energy $\Sigma(\varepsilon_\pm)$ with the help of DMFT+Σ procedure described above, while the nontrivial contribution of disorder scattering enters via $\phi^{0RR(RA)}$ in Eq. (7), which may be calculated in an appropriate approximation. In fact, $\phi^{0RR(RA)}$ contains only disorder scattering, although using the

Green's functions including the DMFT self-energies, already determined with the help of the DMFT+Σ procedure, as the "bare" Green's functions. Equation (6) guarantees the effective interpolation between the case of strong correlations in the absence of disorder and the case of pure disorder in the absence of Hubbard correlations.

The most important $\Phi_{\varepsilon}^{0RA}(\omega,\mathbf{q})$ loop may be calculated using the basic approach of the self-consistent theory of localization [30–35] with some generalizations accounting for the Hubbard interaction within the DMFT+Σ approach [13].

The rest is a direct generalization of the scheme proposed in Ref. [13] for the two-dimensional case. Here, we present only some basic points of the approach in Ref. [13], stressing important differences due to the two-dimensionality of the model.

In the RA channel, the two-particle loop $\Phi_{\varepsilon}^{0RA}(\mathbf{q},\tilde{\omega})$ involves a diffusion-like contribution,

$$\Phi_{\varepsilon}^{0RA}(\mathbf{q},\tilde{\omega}) = \frac{-\sum_{\mathbf{p}} \Delta G_{\mathbf{p}}}{\tilde{\omega} + iD(\omega)q^2}, \tag{9}$$

where $\Delta G_{\mathbf{p}} = G^R(\varepsilon_+,\mathbf{p}) - G^A(\varepsilon_-,\mathbf{p})$. The important difference from the noninteracting case is contained in

$$\begin{aligned}\tilde{\omega} &= \varepsilon_+ - \varepsilon_- - \Sigma^R(\varepsilon_+) + \Sigma^A(\varepsilon_-) = \\ &= \omega - \Sigma^R(\varepsilon_+) + \Sigma^A(\varepsilon_-) \equiv \omega - \Delta\Sigma^{RA}(\omega)\end{aligned} \tag{10}$$

which replaces the usual ω-term in the denominator of the standard expression for $\Phi_{\varepsilon}^{0RA}(\omega,\mathbf{q})$ [35]. Then (6) can be rewritten as

$$\begin{aligned}\operatorname{Re}\sigma(\omega) = \frac{e^2\omega}{2\pi} \int\limits_{-\infty}^{\infty} d\varepsilon\, [f(\varepsilon_-) - f(\varepsilon_+)] \times \\ \times \operatorname{Re}\left\{ \frac{i\sum_{\mathbf{p}} \Delta G_{\mathbf{p}} D(\omega)}{\omega^2} - \right. \\ \left. - \phi_{\varepsilon}^{0RR}(\omega) \left[1 - \frac{\Delta\Sigma^{RR}(\omega)}{\omega}\right]^2 \right\}.\end{aligned} \tag{11}$$

The second term in (11), which is actually irrelevant at small ω, can be obtained from (7) by calculating $\Phi_{\varepsilon}^{0RR}(\omega,\mathbf{q})$ in the usual "ladder" approximation.

Repeating the derivation scheme of the self-consistent theory of localization in Ref. [13], we obtain the following equation for the generalized diffusion coefficient:

$$\begin{aligned}D(\omega) = i\frac{\langle v\rangle^2}{d} \left\{ \tilde{\omega} - \Delta\Sigma_{imp}^{RA}(\omega) + \right. \\ \left. + \Delta^4 \sum_{\mathbf{p}} (\Delta G_{\mathbf{p}})^2 \sum_{\mathbf{q}} \frac{1}{\tilde{\omega} + iD(\omega)q^2} \right\}^{-1},\end{aligned} \tag{12}$$

where $d = 2$ is the spatial dimension and $\Delta\Sigma_{imp}^{RA}(\omega) = \Sigma_{imp}^R(\varepsilon_+) - \Sigma_{imp}^A(\varepsilon_-)$ is determined by disorder scattering. The average velocity $\langle v\rangle$, well approximated by the Fermi velocity, is defined as

$$\langle v\rangle = \frac{\sum_{\mathbf{p}} |\mathbf{v}_{\mathbf{p}}| \Delta G_{\mathbf{p}}}{\sum_{\mathbf{p}} \Delta G_{\mathbf{p}}}, \quad \mathbf{v}_{\mathbf{p}} = \frac{\partial\epsilon(\mathbf{p})}{\partial\mathbf{p}}. \tag{13}$$

Due to the limits of diffusion approximation, the summation over q in (12) must be limited by [33, 35]

$$q < k_0 = \min\{l^{-1}, p_F\} \tag{14}$$

where $l = \langle v\rangle/2\gamma$ is the mean free path due to elastic scattering (γ is the scattering rate due to disorder) and p_F is Fermi momentum. In our two-dimensional model, Anderson localization occurs at infinetisimal disorder. But for small disorder, the localization length is exponentially large, and hence the size of the sample becomes important. The sample size L may be introduced into the self-consistent theory of localization as a cutoff of the diffusion pole contribution at small q [30, 31], i. e., for

$$q \sim k_L = 1/L. \tag{15}$$

Equation (12) for the generalized diffusion coefficient reduces to a transcendental equation, which is easily solved by iterations for each value of $\tilde{\omega}$, taking into account that for $d = 2$ and for the cutoffs defined by Eqs. (14) and (15), the sum over q in (12) reduces to

$$\begin{aligned}\sum_{\mathbf{q}} \frac{1}{\tilde{\omega} + iD(\omega)q^2} = \frac{1}{i2\pi D(\omega)} \times \\ \times \int\limits_{k_L/k_0}^{1} \frac{y\,dy}{y^2 + \tilde{\omega}/iD(\omega)k_0^2} = \\ = \frac{1}{i4\pi D(\omega)} \ln\left(\frac{1 - i\tilde{\omega}/D(\omega)k_0^2}{(k_L/k_0)^2 - i\tilde{\omega}/D(\omega)k_0^2} \right).\end{aligned} \tag{16}$$

Solving Eq. (12) for different values of our model parameters and using Eq. (11), we can directly calculate the optical (dynamic) conductivity in different phases of the Anderson–Hubbard model.

For $\omega \to 0$ (and at the Fermi level ($\varepsilon = 0$), obviously, also $\tilde{\omega} \to 0$), in the Anderson insulator phase,

we obtain the localization behavior of the generalized diffusion coefficient [30, 31, 35]:

$$D(\omega) = -i\tilde{\omega} {R_{loc}}^2. \tag{17}$$

Substituting (17) in (12), we obtain an equation determining the localization length R_{loc} as

$${R_{loc}}^2 = -\frac{\langle v\rangle^2}{d\Delta^4} \times \times \left\{ \sum_{\mathbf{p}} (\Delta G_{\mathbf{p}})^2 \sum_{\mathbf{q}} \frac{1}{1 + {R_{loc}}^2 q^2} \right\}^{-1}, \tag{18}$$

where the sum over q is defined by (16). As we see in what follows, for an infinite two-dimensional system ($L \to \infty$), the localization length determined by Eq. (18) remains finite (although exponentially large) for the smallest possible disorder, signifying the absence of Anderson transition. But for finite-size systems, the localization length diverges at some critical disorder, determined for each value of the system size L. Qualitatively, this critical disorder is determined from the condition of the localization length (in the infinite system) becoming a quantity of the order of the characteristic sample size $R_{loc}^{L\to\infty} \sim L$. Thus, in finite two-dimensional systems, the Anderson transition and the metallic phase do exist for the disorder strength lower than this critical disorder. In what follows, this kind of metallic phase is referred to as the "correlated metal" phase in finite 2D systems.

4. MAIN RESULTS

Below, we present the results of extensive numerical calculations for the 2D Anderson–Hubbard model on a square lattice with a rectangular "bare" DOS corresponding to the bandwidth $W = 2D$:

$$N_0(\varepsilon) = \begin{cases} \dfrac{1}{2D}, & |\varepsilon| \le D \\ 0, & |\varepsilon| > D \end{cases}. \tag{19}$$

The choice of this model DOS is dictated by its 2D nature.

Everywhere in what follows, we give the DOS values in units of the number of states per energy interval, per lattice cell of the volume a^2 (a is the lattice parameter), and per one spin projection.

Because we focus on half-filled case, the Fermi level is always assumed to be at zero energy. As the "impurity solver" for the DMFT effective impurity problem, we use the reliable numerical renormalization group (NRG) approach [27–29]. Calculations were made for the low enough temperature $T \sim 0.001D$, and therefore temperature effects in the DOS and conductivity are negligible.

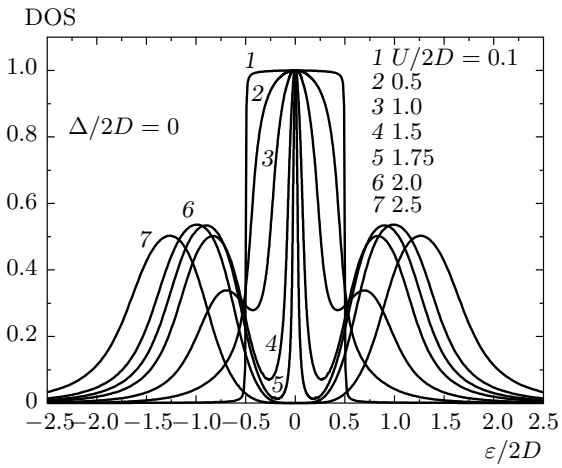

Fig. 2. Density of states of the half-filled Anderson–Hubbard model for different values of U and $\Delta = 0$ (no disorder)

We present only the most typical results.

A. Evolution of the density of states

In Fig. 2, we show the evolution of the DOS with an increase in Hubbard interaction U in the absence of disorder. At small U (curve *1* in Fig. 2), we observe a practically rectangular DOS almost coinciding with the "bare" one. As U increases, a typical three-peak structure of the DOS appears [19, 20, 29] (curves *3*, *4*, and *5* in Fig. 2): a narrow quasiparticle peak at the Fermi level with the upper and lower Hubbard bands at $\varepsilon \sim \pm U/2$. The quasiparticle peak narrows as U increases in the metallic phase, disappearing at the Mott MIT at $U = U_{c2} \approx 1.83$ W. With a further increase in U (curves *6* and *7* in Fig. 2), a dielectric gap opens at the Fermi level.

In Fig. 3, we show the results for the DOS obtained at the relatively weak correlation strength $U = 1.25W$ ($W = 2D$), ensuring that the system is rather far from the Mott transition, but for a wide range of the disorder strength Δ. We observe typical widening of the band with the appropriate suppression of the DOS as disorder increases.

In Fig. 4, the DOS evolution is shown as the disorder Δ increases at $U = 2W$, a typical value for a Mott insulator in the absence of disorder. It can be seen that the increase in disorder leads to the restoration of

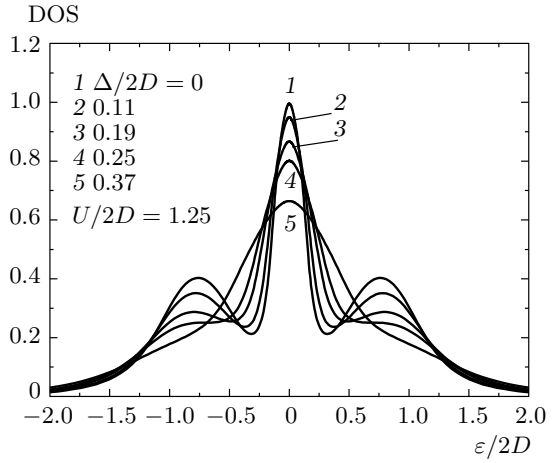

Fig. 3. Density of states of the half-filled Anderson–Hubbard model for different values of disorder Δ and $U/2D = 1.25$, typical for a correlated metal (in the absence of disorder)

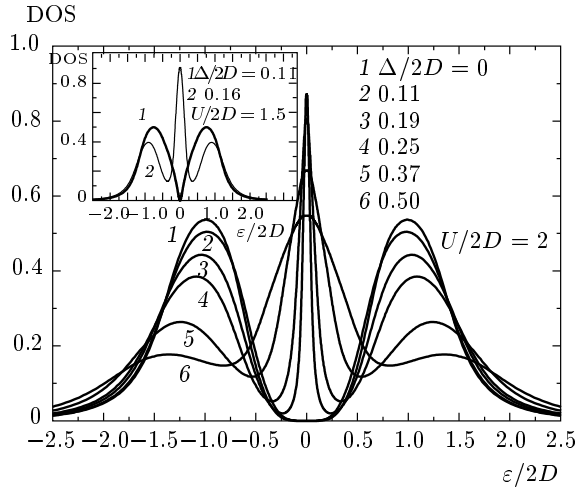

Fig. 4. Density of states of the half-filled Anderson–Hubbard model for different values of disorder Δ and $U/2D = 2$, typical for Mott insulator (in the absence of disorder). At the inset – restoration of quasiparticle band by disorder in coexistence (hysteresis) region for $U = 1.5D$, obtained from Mott insulator with decreasing U

the quasiparticle peak in the DOS. A similar unusual behavior of the DOS (closure of the dielectric gap by disorder) was first noted in 3D systems [13]. But in the present 2D case, it does not, in general, signify the transition to the correlated metal phase, at least for the infinite systems we are in fact dealing with intems of the correlated Anderson insulator (see below).

The physical reason for this unusual restoration of the quasiparticle peak in the DOS is clear. The control parameter for the appearance or disappearance of a quasiparticle peak in DMFT in the absence of disorder is the ratio of the Hubbard interaction U to the "bare" bandwidth $W = 2D$. Disordering leads to an increase in the effective bandwidth W_{eff} (in the absence of the Hubbard interaction) and the appropriate suppression of the U/W_{eff} ratio, which obviously leads to a restoration of the quasiparticle band in our model. In more detail, this qualitative picture is discussed in Sec. 4C, where our results for the DOS are used in constructing the phase diagram of the 2D Anderson–Hubbard model.

It is well known, that hysteresis behavior of DOS is obtained for Mott–Hubbard transition if we perform DMFT calculations with U decreasing from insulating phase [20, 29]. Mott insulator phase survives for the values of U well inside the correlated metal phase, obtained with the increase of U. Metallic phase is restored at $U_{c1} \approx 1.42W$. The values of U from the interval $U_{c1} < U < U_{c2}$ are usually considered as belonging to coexistence region of metallic and (Mott) insulating phases, with metallic phase being thermodynamically more stable [20, 29]. In the coexistence region disorder increase also leads to the restoration of quasiparticle peak in the DOS (see inset of Fig. 4).

B. Optical conductivity: Mott–Hubbard and Anderson transitions

The real part of the optical conductivity was calculated for different combinations of parameters of the model, directly from Eqs. (11) and (12) using the results of the DMFT+Σ procedure for single-particle characteristics. The values of conductivity below are given in natural units of $e^2/\hbar$.

In the absence of disorder, we just reproduce the results of the standard DMFT with the optical conductivity characterized by the usual Drude peak at zero frequency and a wide maximum at $\omega \sim U$ corresponding to transitions to the upper Hubbard band. As U increases, the Drude peak is suppressed and disappears at the Mott MIT, when the only remaining contribution is due to transitions through the Mott–Hubbard gap.

Introduction of disorder leads to a qualitative change in the frequency behavior of conductivity. Below, we mainly present the results obtained for the same values of U and Δ that were used above to illustrate the evolution of the DOS.

In Fig. 5, we show the real part of the optical conductivity in the 2D half-filled Anderson–Hubbard model for different disorder strengths Δ and

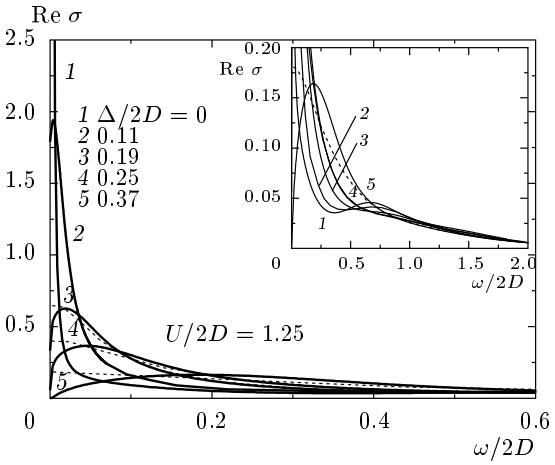

Fig. 5. Real part of the dynamic conductivity of the half-filled Anderson–Hubbard model for different values of disorder Δ and $U/2D = 1.25$, typical for a correlated metal (in the absence of disorder). Inset: the same, but in a wider frequency range. Thin dashed lines represent the ladder approximation results

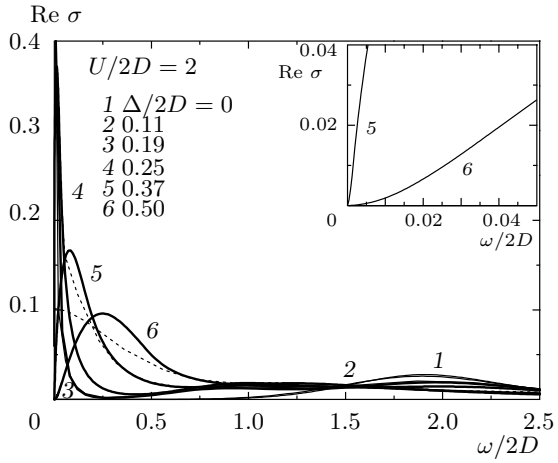

Fig. 6. Real part of the dynamic conductivity of the half-filled Anderson–Hubbard model for different values of disorder Δ and $U/2D = 2$, typical for Mott insulator (in the absence of disorder). Curves *1* and *2* correspond to a Mott insulator, and curves *3*–*6* correspond to a correlated Anderson insulator. Inset: localization behavior of conductivity. Thin dashed lines are the ladder approximation results

$U = 1.25W$, when the system is far from the Mott MIT. Thin dashed lines in Fig. 5 (and in the following figures) show the results of the "ladder" approximation. In the 2D model under consideration, the conductivity at zero frequency is always zero, and in contrast to the 3D case [13], even for the weakest possible disorder, the peak in the optical conductivity is at a finite frequency. In the "ladder" approximation, which does not contain localization corrections, the conductivity is finite at $\omega = 0$. Optical transitions to the upper Hubbard band at $\omega \sim U$ are practically unobservable in these data; only in the inset to Fig. 5, where we show the data for the wide frequency range, a weak maximum on curves *1* and *2* can be observed, corresponding to transitions to the upper Hubbard band.

In Fig. 6, we present the real part of the optical conductivity for different disorder strengths Δ and $U = 2W$, typical for a Mott insulator. It can be seen from Fig. 6 that for small disorder, we are in the Mott insulator phase (curves *1* and *2*), and with an increase in disorder in the absence of Anderson localization (cf. the thin lines corresponding to the "ladder" approximation), we would be entering the metallic phase. But in our model, localization occurs at infinitesimal disorder and we are actually entering Anderson insulator phase, with the conductivity ending to zero at zero frequency. Data in the frequency range corresponding to the localization behavior $\sigma(\omega) \propto \omega^2$ of conductivity are shown at the inset to Fig. 6 for curves *5* and *6*, corresponding to a large enough disorder. At small disorders, the frequency region with the localization behavior of the conductivity is exponentially small[1)] (which is due to the exponential increase in the localization length at small disorder, cf. Fig. 9) and is practically unobservable.

The dependence of the optical conductivity on U is illustrated in Fig. 7. The increase in U shifts the localization peak in the conductivity to lower frequencies and leads to its narrowing. Apparently, this is related to the appropriate suppression of the quasiparticle peak width in DOS. The value of conductivity at the maximum is independent of U. It is interesting to note that for frequencies larger than the maximum position, the increase in U suppresses conductivity, while for the frequencies lower than the maximum position, the increase in U enhances conductivity (in a sense, playing against localization).

To confirm the self-consistency of our approach to conductivity calculations, we conclude this section with a discussion of the optical sum rule, which relates single-particle and two-particle characteristics [36].

[1)] This region corresponds to frequencies $\omega \ll \omega_c \sim \sim \frac{D^3}{\Delta^2} / \left(\frac{R_{loc}}{a}\right)^2$ [30, 31].

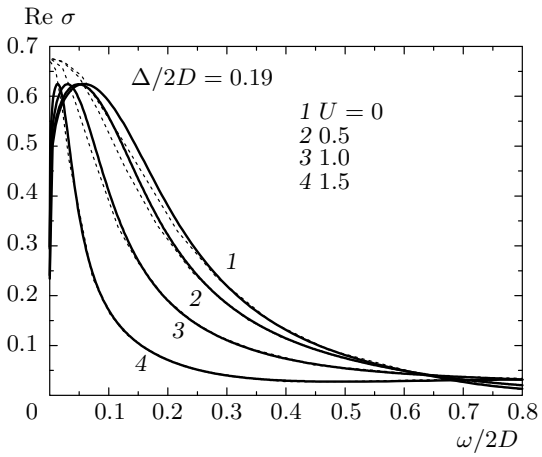

Fig. 7. Real part of the dynamic conductivity of the half-filled Anderson–Hubbard model for different values of U and $\Delta/2D = 0.19$. Thin dashed lines are ladder approximation results

Table. Check of the single-band optical sum rule in the Anderson–Hubbard model. The optical integral is given in units of $2e^2D/\hbar$

$\Delta/2D$	$\pi e^2/2 \sum_{\mathbf{p}} \partial^2\varepsilon_p/\partial p_x^2 n_p$	$W_{opt} = \int_0^\infty \mathrm{Re}\,\sigma(\omega)\,d\omega$
0.19	0.099	0.098
0.25	0.099	0.098
0.37	0.092	0.091
0.5	0.081	0.082

The single-band Kubo sum rule [37] for the dynamic conductivity can be written as

$$W_{opt} = \int_0^\infty \mathrm{Re}\,\sigma(\omega)\,d\omega = \frac{\pi e^2}{2} \sum_{\mathbf{p}} \frac{\partial^2 \varepsilon_p}{\partial p_x^2} n_p, \qquad (20)$$

where n_p is the single-particle momentum distribution function, determined by the interacting retarded electron Green's function $G^R(\varepsilon, \mathbf{p})$:

$$n_p = -\frac{1}{\pi} \int_{-\infty}^{\infty} d\varepsilon\, f(\varepsilon) Im G^R(\varepsilon, \mathbf{p}), \qquad (21)$$

where $f(\varepsilon)$ is the Fermi distribution.

In Table, we show calculated values of the right-hand side and of the left-hand side of Eq. (20) for $U = 1.5W$. It is clearly seen that optical sum rule (20) is fulfilled within our numerical accuracy.

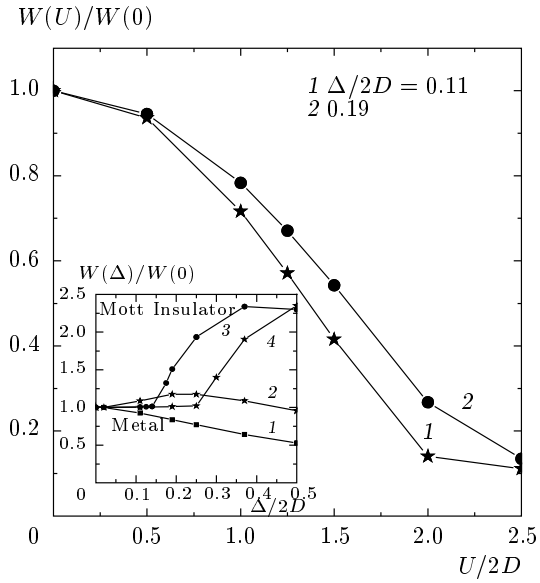

Fig. 8. Dependence of the normalized optical integral of the Anderson–Hubbard model on U for different values of disorder Δ. Inset: a similar dependence on Δ for different values of U ($U/2D = 1$ (curve *1*), 1.5 (*2*), 2 (*3*), 2.5 (*4*)). Curves *1* and *2* pertain to a "correlated metal" transforming into the Anderson insulator. Curves *3* and *4* are a Mott insulator, obtained as U increases from "correlated metal" or Anderson insulator value

Very often, the optical sum rule is understood as the equality of the optical integral W_{opt} to the "universal" value of $\omega_{pl}^2/8$, where ω_{pl} is the plasma frequency, which, strictly speaking, is not correct in the single-band case; in this sense, we may speak of an optical sum rule "violation". In fact, the optical integral depends on parameters of the model, e. g., on the Hubbard interaction and disorder (Fig. 8). The increase in U significantly suppresses the value of the optical integral. The dependence on the disorder strength Δ is also important; in particular, under a disorder-induced transition from the Mott to the Anderson insulator, we observe a kind of discontinuity of the optical integral (curves *3* and *4* at the inset to Fig. 8).

C. Localization length and phase diagram of the 2D Anderson–Hubbard model

To proceed, on the left axis in Fig. 9 we present our data for the real part of the conductivity at a fixed and sufficiently small frequency $\omega = 0.00005D$ plotted as a function of the disorder strength Δ. Circles show the results of "ladder" approximation, and triangles, the results of the self-consistent theory of localization

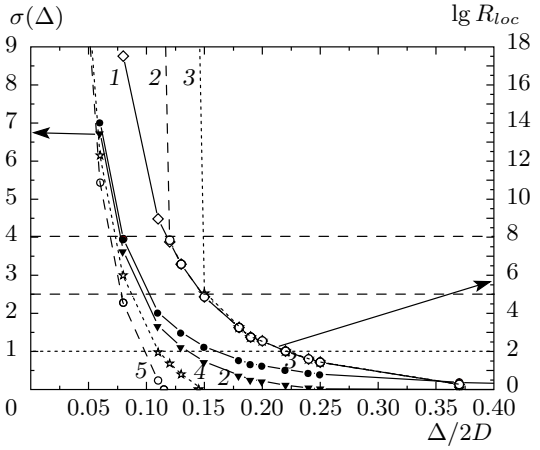

Fig. 9. Left scale shows the dependence of conductivity on disorder Δ at the fixed frequency $\omega = 0.00005D$ and $U/2D = 1$. Circles (curve *1*) — ladder approximation; triangles (curve *2*) — self-consistent theory of localization. Curve *3*, practically coinciding with the ladder approximation results, is obtained from Drude expression (22). Static conductivity for finite samples of sizes $L = 10^8 a$ (curve *4*) and $L = 10^5 a$ (curve *5*). Right scale shows the dependence of the localization length logarithm on disorder Δ for an infinite sample (curve *1*) and for finite samples of sizes $L = 10^8 a$ (curve *2*) and $L = 10^5 a$ (curve *3*)

(we take $U = 0$ here). Curve *3*, which practically coincides with the results of the "ladder" approximation, is obtained from the usual Drude expression

$$\sigma(\omega) = \sigma(0)\frac{\gamma^2}{\gamma^2 + \omega^2}, \tag{22}$$

where the static conductivity is given by

$$\sigma(0) = e^2 N(0) D_0 \approx \frac{e^2}{\hbar}\,\frac{\varepsilon_F}{2\pi\gamma},$$

with $N(0)$ being the density of states at the Fermi level, D_0 the classical diffusion coefficient, and $\varepsilon_F \approx D$ the Fermi energy. The impurity scattering rate was taken as

$$\gamma = \pi N(0)\Delta^2 \approx \frac{\pi}{2D}\Delta^2.$$

It can be seen that a noticeable contribution of localization corrections to conductivity (the clear difference between curve *2* and curves *1* and *3*) appears only after the conductivity decreases below the values of the order of the "minimal" metallic conductivity $\sigma_0 = e^2/\hbar$ (our data for conductivity are actually normalized by this value in all figures). We see below that precisely in this region, a kind of Anderson MIT (divergence of the localization length) occurs in 2D systems of reasonable finite sizes.

On the right axis in Fig. 9, we show our data for the logarithm of the localization length calculated from Eq. (18) as a function of disorder for an infinite sample (curve *1*) and for finite samples with $L = 10^8 a$ and $L = 10^5 a$ (curves *2* and *3*). It is clearly seen that the localization length increases exponentially as the disorder decreases, but remains finite in the infinite 2D sample, signifying the absence of the Anderson transition. In finite samples, the localization length diverges at some critical disorder (depending on the system size), demonstrating the existence of an effective Anderson transition. It follows from Fig. 9 that this critical disorder is achieved when the localization length of an infinite system becomes comparable to the characteristic size of the sample: $R_{loc}^{L\to\infty} \sim L$. We note that in our approach, in contrast to the results in Ref. [15], the localization length is practically independent of U, which leads to the independence of the critical disorder in 2D from the correlation strength U. A similar result[2)] was obtained in our approach for 3D systems [13].

On the left axis in Fig. 9, the disorder dependence of the static conductivity for finite samples of the sizes $L = 10^8 a$ and $L = 10^5 a$ (curves *4* and *5*) is shown. For finite systems with small disorder, the static conductivity is not zero (metal). It gradualy decreases as the disorder increases and becomes zero at the same critical value where the localization radius diverges on approach from the insulating phase in a finite sample. The static conductivity of finite samples in our calculations is practically independent of the correlation strength U. A rather significant difference between the values of static conductivity and that of conductivity at small but nonzero frequencies seen in Fig. 9 comes from the exponential smallness of the frequency range of localization behavior mentioned above.

We now discuss our results for the phase diagram of the 2D half-filled Anderson–Hubbard model, obtained from extensive DMFT+Σ calculations of the DOS and the analysis of the localization length behavior in finite 2D systems. The general form of this phase diagram in the disorder–correlation (Δ, U) plane is shown in Fig. 10.

The dashed stripe in Fig. 10 corresponds to the region of an effective transition from the Anderson insulator to the "metallic" phase. Its boundaries were determined by divergence of the localization length in

[2)] Our calculations of the localization length for a 3D system performed after the publication of Ref. [13] have demonstrated that it is practically independent of the value of U.

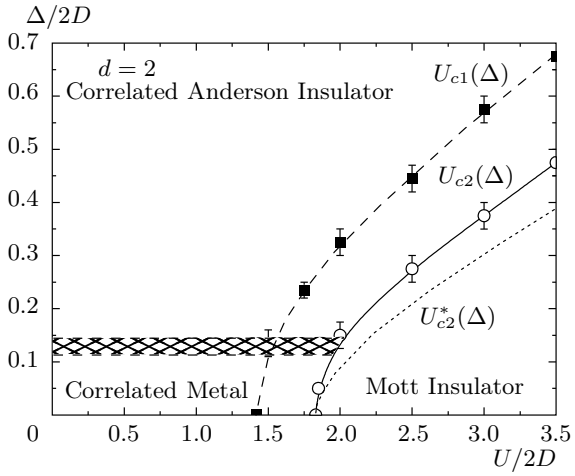

Fig. 10. Phase diagram of the two-dimensional paramagnetic Anderson–Hubbard model at zero temperature. The border of Mott insulator region $U_{c2}(\Delta)$ and the border of coexistence (hysteresis) region $U_{c1}(\Delta)$ are obtained from the evolution of the density of states, and $U^*_{c2}(\Delta)$ is calculated from (24). The dashed stripe corresponds to the narrow region where the Anderson metal–insulator transition occurs in finite systems

finite samples with characteristic sizes $L = 10^5 a$ (upper boundary) and $L = 10^8 a$ (lower boundary) (cf. Fig. 9). We stress that a further increase in the system size, e. g., 10 times up to $L = 10^9 a$, leads only to a practically negligible downshift of the lower boundary (decrease in the critical disorder) of the dashed stripe in Fig. 10.

The dependence of $U_{c2}(\Delta)$ obtained from the DOS behavior determines the boundary for the Mott transition and is defined by the disappearance of the quasiparticle peak in the DOS and by correlation gap opening at the Fermi level (cf. Figs. 2, 4).

In our previous work [13] on the 3D Anderson–Hubbard model, we proposed a simple explanation of the $U_{c1,c2}(\Delta)$ dependence. Assuming that the controlling parameter of the Mott–Hubbard transition, given by the ratio $U_{c1,c2}(\Delta)/W_{eff}(\Delta)$ of the Hubbard interaction to the effective bandwidth (depending on disorder), is a universal constant (independent of disorder), we obtain

$$\frac{U_{c1,c2}(\Delta)}{W_{eff}(\Delta)} = \frac{U_{c1,c2}(0)}{W}, \qquad (23)$$

where $W_{eff}(\Delta)$ is an effective bandwidth in the presence of disorder, calculated at $U = 0$ in self-consistent Born approximation (5). In the 3D model [13], the dependence of the critical correlation strength on disorder $U_{c1,c2}(\Delta)$, obtained directly from the evolution of the DOS, has shown a quite satisfactory agreement with the qualitative dependence obtained from Eq. (23)[3)].

In the 2D model under consideration here, a solution of Eq. (23) gives

$$U^*_{c1,c2}(\Delta) = U_{c1,c2}(0)\frac{W_{eff}(\Delta)}{W} = \\ = U_{c1,c2}(0)\left(\frac{2\Delta^2}{W^2}\ln\left(\frac{c+1}{c-1}\right) + c\right), \qquad (24)$$

where $c = \sqrt{4\left(\Delta/W\right)^2 + 1}$. However, unlike in the 3D case [13], the $U_{c2}(\Delta)$ dependence obtained from the DOS evolution is clearly different from the qualitative dependence $U^*_{c2}(\Delta)$ (the dotted line in Fig. 10), determined by Eq. (24). Probably, this is due to a significant change in the rectangular form of the "bare" DOS with an increase in the disorder Δ, which is absent for the semi-elliptic "bare" DOS used in the 3D case in Ref. [13].

As we already noted, with decrease of U from insulating phase Mott transition occurs at $U = U_{c1}(\Delta) < U_{c2}(\Delta)$ and the coexistence (hysteresis) region is observed between $U_{c1}(\Delta)$ and $U_{c2}(\Delta)$ curves on phase diagram Fig. 10.

5. CONCLUSION

We have used the generalized DMFT+Σ approach to study basic properties of the disordered and correlated Anderson–Hubbard model. Our method produces a relatively simple interpolation scheme between two well-studied limits, the strongly correlated Hubbard model in the absence of disorder (DMFT and Mott–Hubbard MIT) and the 2D Anderson insulator in the infinite system without electron–electron interactions. It seems that the proposed interpolation scheme reflects all the qualitative features of the Anderson–Hubbard model, such as the behavior of the density of states and dynamic conductivity. The general structure of the phase diagram obtained in the DMFT+Σ approximation is also in reasonable agreement with the results of direct numerical simulations [16]. At the same time, the DMFT+Σ approach is rather competitive in the sense of the amount of numerical work and allows direct calculations of all the basic observable characteristics of the Anderson–Hubbard model.

[3)] Further extensive calculations performed after the completion of Ref. [13] have confirmed a practically ideal agreement between these dependences.

We stress that an effective Anderson transition obtained here in the case of finite-size 2D systems is in no sense attributed to electronic correlations and also follows directly from the self-consistent theory of localization in the absence of correlations.

The main shortcoming of the method used is the neglect of the interference between disorder scattering and Hubbard interaction, which leads to the independence of the localization length and critical disorder Δ_c (in finite 2D systems) from the correlation strength U. The importance of this kind of interference effects has been known since long ago [1, 5], although these can be taken into account only in the case of weak correlations and disorder. At the same time, the neglect of the interference effects is the key point of our DMFT+Σ approach, which allows obtaining rather simple and physically clear interpolation scheme and analyzing the limits of strong correlations and disorder.

Another drastic simplification is our assumption of a nonmagnetic (paramagnetic) nature of the ground state of the Anderson–Hubbard model. The importance of magnetic (spin) effects in strongly correlated and disordered systems is obvious, as is the importance of competition between different kinds of magnetic ground states [20].

Despite these shortcomings, our results seem rather attractive and reliable, e. g., with respect to strong disorder effects on the Mott–Hubbard transition and the general form of the phase diagram at $T = 0$. Our predictions for the general behavior of the dynamic (optical) conductivity and the disorder-induced Mott insulator to the effective "metal" transition can be directly compared with the existing and future experiments.

We are grateful to Th. Pruschke for providing us with his effective NRG code.

This work was supported in part by the RFBR grant 08-02-00021 and programs of fundamental research of the Presidium of RAS "Quantum physics of condensed state" and that of Physics Department of RAS "Strongly correlated electrons in solids", as well as by the grant of the President of Russian Federation MK-614.2009.2 (I. A. N.).

REFERENCES

1. P. A. Lee and T. V. Ramakrishnan, Rev. Mod. Phys. **57**, 287 (1985); D. Belitz and T. R. Kirkpatrick, Rev. Mod. Phys. **66**, 261 (1994).
2. E. Abrahams, P. W. Anderson, D. C. Licciardello, and T. V. Ramakrishnan, Phys. Rev. Lett. **42**, 673 (1979).
3. B. L. Altshuler, A. G. Aronov, and P. A. Lee, Phys. Rev. Lett. **44**, 1288 (1980).
4. G. J. Dolan and D. D. Osheroff, Phys. Rev. Lett. **43**, 721 (1979); D. J. Bishop, D. C. Tsui, and R. C. Dynes, Phys. Rev. Lett. **44**, 1153 (1980); M. J. Uren, R. A. Davies, and M. Pepper, J. Phys. C **13**, L985 (1980).
5. A. M. Finkelshtein, Sov. Phys. JETP **75**, 97 (1983); C. Castellani et al., Phys. Rev. B **30**, 527 (1984).
6. S. V. Kravchenko and M. P. Sarachik, Rep. Prog. Phys. **67**, 1 (2004).
7. E. Abrahams, S. V. Kravchenko, and M. P. Sarachik, Rev. Mod. Phys. **73**, 251 (2001)
8. N. F. Mott, Proc. Phys. Soc. A **62**, 416 (1949); *Metal–Insulator Transitions*, 2nd edn., Taylor and Francis, London (1990).
9. P. W. Anderson, Phys. Rev. **109**, 1492 (1958).
10. V. Dobrosavljević and G. Kotliar, Phys. Rev. Lett. **78**, 3943 (1997).
11. V. Dobrosavljević, A. A. Pastor, and B. K. Nikolić, Europhys. Lett. **62**, 76 (2003).
12. K. Byczuk, W. Hofstetter, and D. Vollhardt, Phys. Rev. Lett. **94**, 056404 (2005).
13. E. Z. Kuchinskii, I. A. Nekrasov, and M. V. Sadovskii, Zh. Eksp. Teor. Fiz. **133**, 670 (2008).
14. P. Henseler, J. Kroha, and B. Shapiro, Phys. Rev. B **77**, 075101 (2008).
15. P. Henseler, J. Kroha, and B. Shapiro, Phys. Rev. B **78**, 235116 (2008).
16. M. E. Pezzoli and F. Becca, arXiv:0906.4870.
17. W. Metzner and D. Vollhardt, Phys. Rev. Lett. **62**, 324 (1989).
18. D. Vollhardt, in *Correlated Electron Systems*, ed. by V. J. Emery, World Scientific, Singapore (1993), p. 57.
19. Th. Pruschke, M. Jarrell, and J. K. Freericks, Adv. Phys. **44**, 187 (1995).
20. A. Georges, G. Kotliar, W. Krauth, and M. J. Rozenberg, Rev. Mod. Phys. **68**, 13 (1996).
21. M. Ulmke, V. Janiš, and D. Vollhardt, Phys. Rev. B **51**, 10411 (1995).

22. R. Vlaming and D. Vollhardt, Phys. Rev. B **45**, 4637 (1992).

23. E. Z. Kuchinskii, I. A. Nekrasov, and M. V. Sadovskii, Pis'ma v Zh. Eksp. Teor. Fiz. **82**, 217 (2005).

24. M. V. Sadovskii, I. A. Nekrasov, E. Z. Kuchinskii, Th. Prushke, and V. I. Anisimov, Phys. Rev. B **72**, 155105 (2005).

25. E. Z. Kuchinskii, I. A. Nekrasov, and M. V. Sadovskii, Fizika Nizkikh Temperatur **32**, 528 (2006).

26. E. Z. Kuchinskii, I. A. Nekrasov, and M. V. Sadovskii, Phys. Rev. B **75**, 115102 (2007).

27. K. G. Wilson, Rev. Mod. Phys. **47**, 773 (1975); H. R. Krishna-murthy, J. W. Wilkins, and K. G. Wilson, Phys. Rev. B **21**, 1003 (1980); **21**, 1044 (1980); A. C. Hewson, *The Kondo Problem to Heavy Fermions*, Cambridge University Press, Cambridge (1993).

28. R. Bulla, A. C. Hewson, and Th. Pruschke, J. Phys.: Condens. Matter **10**, 8365 (1998).

29. R. Bulla, Phys. Rev. Lett. **83**, 136 (1999); R. Bulla, T. A. Costi, and D. Vollhardt. Phys. Rev. B **64**, 045103 (2001).

30. D. Vollhardt and P. Wölfle, Phys. Rev. B **22**, 4666 (1980); Phys. Rev. Lett. **48**, 699 (1982)

31. P. Wölfle and D. Vollhardt, in *Anderson Localization*, ed. by Y. Nagaoka and H. Fukuyama, Springer Series in Solid State Sciences, Vol. 39, Springer-Verlag, Berlin (1982), p. 26.

32. A. V. Myasnikov and M. V. Sadovskii, Fiz. Tverd. Tela **24**, 3569 (1982); E. A. Kotov and M. V. Sadovskii, Z. Phys. B **51**, 17 (1983).

33. M. V. Sadovskii, in *Soviet Scientific Reviews–Physics Reviews*, ed. by I. M. Khalatnikov, Vol. 7, Harwood Academic Publ., New York (1986), p. 1.

34. D. Vollhardt and P. Wölfle, in *Electronic Phase Transitions*, ed. by W. Hanke and Yu. V. Kopaev, Vol. 32, North–Holland, Amsterdam (1992), p. 1.

35. M. V. Sadovskii, *Diagrammatics*, World Scientific, Singapore (2006).

36. E. Z. Kuchinskii, N. A. Kuleeva, M. V. Sadovskii, and I. A. Nekrasov, Zh. Eksp. Teor. Fiz. **107**, 281 (2008).

37. R. Kubo, J. Phys. Soc. Jpn. **12**, 570 (1957).